IEEE Access
Multidisciplinary ⋮ Rapid Review ⋮ Open Access Journal

Received December 13, 2020, accepted January 8, 2021, date of publication February 9, 2021, date of current version February 18, 2021.

Digital Object Identifier 10.1109/ACCESS.2021.3058089

Partial Discharge Phenomena in Electrical Machines for the More Electrical Aircraft. Part II: Impact of Reduced Pressures and Wide Bandgap Devices

LUCA LUSUARDI[1], (Member, IEEE), ALBERTO RUMI[2], (Student Member, IEEE), ANDREA CAVALLINI[2], (Senior Member, IEEE), DAVIDE BARATER[3], (Member, IEEE), AND STEFANO NUZZO[3], (Member, IEEE)

[1]Thyssenkrupps Presta AG, 9492 Eschen, Liechtenstein
[2]Department of Electrical, Electronic and Information Engineering "Guglielmo Marconi," University of Bologna, 40136 Bologna, Italy
[3]Department of Engineering "Enzo Ferrari," University of Modena-Reggio Emilia, 41125 Modena, Italy

Corresponding author: Stefano Nuzzo (stefano.nuzzo@unimore.it)

This work was supported by the Reliable Aircraft electrical Insulation System sElection (RAISE) project through the Clean Sky 2 Joint Undertaking under the European Union's Horizon 2020 Research and Innovation Programme under Grant 785513.

ABSTRACT This paper focuses on the inception of partial discharges within the insulation system of electrical actuators used for the More Electrical Aircraft (MEA). Since these machines should operate in the absence of Partial Discharges (PDs), the dependence of the PD Inception Voltage (PDIV) on voltage impulses typical of wide bandgap (SiC) devices is investigated at both 1 bar, reduced pressures close to those typical of aircraft cruising altitudes (150 mbar – 200 mbar) or lower (down to 5 mbar). Propagation issues are not dealt with here as results were obtained working on insulation models consisting of couples of wires twisted together (twisted pairs), thus knowing exactly the potential differences between all points of the insulation model. The results show that the rise times and the switching frequencies associated with wide bandgap devices have little impact on the PDIV. A model able to predict the PDIV of the turn/turn insulation of random wound motors (the most vulnerable part of the insulation) at different pressures is proposed. The model is also able to deal with temperature changes, with limitations that depend on the type on insulation systems.

INDEX TERMS Partial discharges, more electrical aircraft, MEA, wide bandgap devices, SiC inverter, qualification.

I. INTRODUCTION

Power converters based on wide bandgap devices (silicon carbide, SiC, and gallium nitride, GaN) are attractive for manufacturing the More Electrical Aircraft (MEA) [1]–[4]. Compared to standard silicon devices, SiC switches can operate at higher electrical fields and temperatures. Thanks to the very short turn on and off times (10-20 ns), they can attain $\times 100$ kHz switching frequencies. These features allow to build actuators operating at higher voltages and higher modulating frequencies, thus achieving large power densities, something that is highly desirable for the MEA.

The associate editor coordinating the review of this manuscript and approving it for publication was Jenny Mahoney.

These advantages come at a cost. The interactions between power converters and motors raise the electrical stress on the motor insulation [5], [6]. On one side, the voltage impulses of the converter get reflected at the motor terminals since the cable characteristic impedance is lower than the surge impedance of the stator. In the worst case, the voltage at the motor terminals can be twice the DC bus voltage. On the other side, since the windings are a complex inductive/capacitive network, during the voltage impulses flanks, most of the line voltage drops on few turns close to the terminals. For random wound motors, there is a concrete risk that, in the coil connected to the line terminal, two turns having a potential difference comparable to the phase-to-ground voltage are in contact, leading to a high electrical stress. Compared to

conventional silicon switches, SiC exacerbate these phenomena as reflections can occur with very short cables and the turn voltage distribution becomes even more uneven [7], [8].

These factors can raise the electrical stress above a critical field, leading to partial discharge (PD) inception. PDs are localized discharges that do not bridge the insulation [9]. However, their prolonged activity causes a progressive deterioration which leads to breakdown. The PD repetition rate is very high under power converters since a PD event is likely to take place at both flanks of the voltage impulses. Considering that SiC switching frequencies can be as large as 100 kHz, failure can occur in short times, e.g. a few minutes, because of the organic nature of the insulation [10]–[12].

Avoiding partial discharge inception long enough to ensure the reliability of the drive is sometimes difficult for motors used in industrial drives [13]. Particularly critical in this respect is the turn/turn insulation, where winding wires are in contact and the insulation thickness is only few tens of μm. This is typically the point where failures occur. When considering aircraft actuators, the challenges are far more pressing as the low pressure at cruising altitudes reduces the PD inception voltage (PDIV), [14]–[17]. One of the open points is understanding whether high frequency and high dV/dt impulses can have an impact on the physics of PDs leading to a further reduction of PDIV. The impact of atmospheric conditions typical of the MEA should also be evaluated in conjunction with high dV/dt impulses.

This paper discusses the relationship between PD phenomena and voltage waveforms typical of SiC inverters considering reduced atmospheric pressures. The focus is on the turn/turn insulation of random wound motors, which is the most critical one for this type of machines. Insulation models used in the investigation are winding wires twisted together (twisted pairs). The field in these models follows a capacitive distribution. Thus, the conclusions reached are not related to propagation in a complex system but to the physics of the discharge at distinct pressures, temperature, voltage rise time and frequency.

This paper is organized as follows. Section II presents the test setup (test cell, high voltage sources, and PD sensors). The MEA atmospheric conditions and the supply voltage waveforms affect the detectability of PD [18], [19]. Thus, Section III reports pros and cons of the different detection systems depending on the features of the high voltage source. This discussion could interest in view of monitoring PDs in aircraft. Section IV presents the experimental results and introduces an empirical model to predict the PDIV as a function of both pressure and temperature. Section V shows that the model holds for a vast class of insulation models. Section VI concludes summarizing the results and offering a perspective on the application of the results.

II. EXPERIMENTAL SETUP

The test setup was realized for testing insulation models (twisted pairs) subjected to both AC sinusoidal voltages and large slew rate (up to 140 kV/μs) bipolar voltage impulses. A vacuum cell able to reach pressures down to 1 mbar coupled with a heating system was used to simulate atmospheric conditions typical of an MEA actuator. Three different detection systems were used: conventional, optical, and UHF. Under voltage impulses only UHF and optical detection systems can be used due to the inverter interference [20]–[22]. Their relative sensitivities will be discussed in the next section. The conventional system was used with sinusoidal voltages to test the relative sensitivities of the alternative detection systems.

A. TEST SAMPLES

Grade 2 round enameled wires having a diameter of 0.63 mm were used in the experiments. The insulation is in thermal class 200, and it features a THEIC-modified polyester-imide basecoat and a polyamide-imide overcoat. According to [23], the wires were twisted 12 times applying a load of 7 N. For each test condition, 10 freshly manufactured twisted pairs were used. After each test, the twisted pair were discarded. The 10th percentile (B10) of the Weibull distribution fitting the experimental data is used to synthesize the PDIV values.

B. HV SOURCES

Distinct voltage sources were used for the investigation. The first voltage source is a step-up 220/3000 V transformer controlled by a 220:220 V autotransformer on the low voltage winding. This source was used to measure PDIV under 50 Hz sinusoidal voltages. The effect of sinusoidal voltages having higher frequencies was tested using a resonant HV source capable of working at frequencies of 40 kHz with a maximum voltage of 10 kV. The source was manufactured by the University of Bologna.

A SiC inverter was designed and assembled by the University of Modena. The inverter is based on Wolfspeed C2M1000170D SiC MOSFETs. These MOSFETs have a blocking voltage of 1700 V. The lowest rise time of the MOSFETs is 7 ns corresponding to a gate resistance of 27 Ω. To test with lower slew rates, gate resistances of 53 Ω and 500 Ω were used to achieve rise times of 15 ns and 150 ns, respectively. Tests were carried out at switching frequencies reaching 100 kHz with variable rise times.

The voltage applied to the pass-throughs of the test cell was measured by Tektronix MDO3054D oscilloscope (500MHz bandwidth, 2.5GS/s sampling rate) using a Tektronix THDP0200 differential probe (200 MHz bandwidth). The voltage waveforms provided by the SiC inverter are shown in FIGURE 1. Only for the lowest rise time the overshoot is significant (67%).

C. TEST CELL

A test cell was manufactured to carry out high voltage tests in a partial vacuum. The test cell is a sealed cylindrical vacuum tank (internal diameter 220 mm, height 310 mm), see FIGURE 2, and is equipped with 20 kV high voltage pass-throughs on the top lid, three optical windows, four BNC pass-throughs to monitor physical quantities within the tank (see FIGURE 3). To make sure an optical path from the

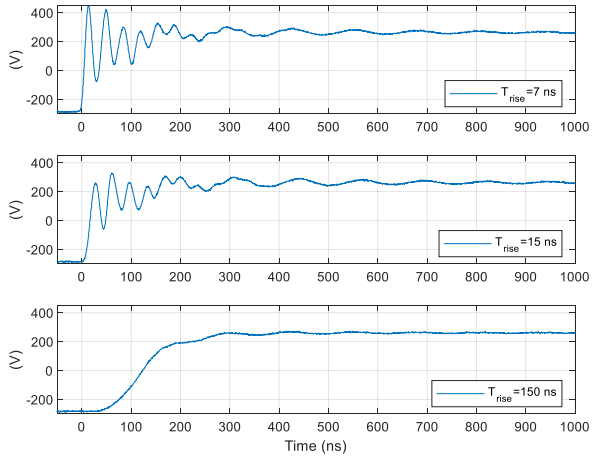

FIGURE 1. SiC Inverter waveforms having different rise times.

FIGURE 2. Picture of the test cell.

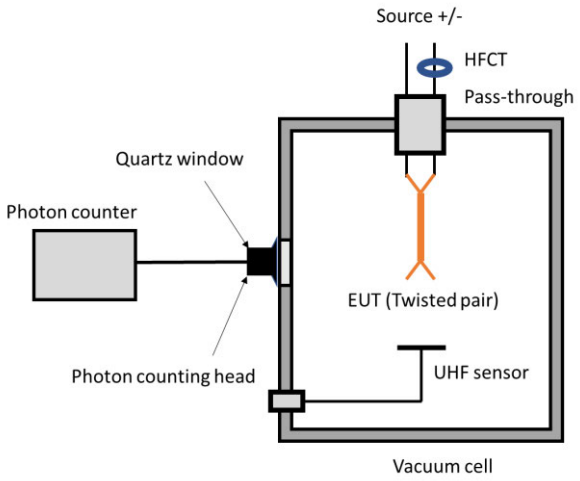

FIGURE 3. Sketch of the test cell equipped with PD detection system.

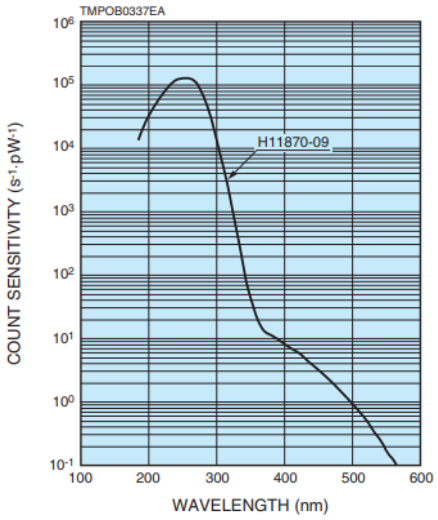

FIGURE 4. Photon counting head count sensitivity [24].

discharge site to an optical PD detection system (described below), the windows are placed around the Equipment Under Test (EUT).

The pressure was reduced using a rotary pump. It was monitored using a digital vacuum gauge. The tightness of the cell ensured that the pressure did not raise over 1 mbar in 20 minutes, long enough to do the measurements.

A custom-made heater was manufactured to carry out tests at controlled temperature and reduced pressures. The heater comprises a copper wire coiled on a refractory support and fed by a high DC current (40 A) supply system. The heater was calibrated prior the tests by placing thermocouples 10 mm from a twisted pair. For different current magnitudes, the temperatures on the sample and on the copper wire were measured. This procedure was carried out at the different pressure levels chosen for testing (thus under different heat exchange conditions) and up to 120°C. During the tests, the temperature of the test object was maintained at the desired level by a PID controller using as a feedback signal the temperature of the air at 10 mm from the twisted pair.

D. PARTIAL DISCHARGE DETECTION SYSTEM

To detect PDs, the test cell was equipped with optical, UHF, and conventional (based on conducted currents, [9]) PD detection systems as sketched in FIGURE 3.

Optical partial discharge detection is achieved using a photon-counting system. It comprises two pieces manufactured by Hamamatsu Photonics: (a) a H11870-09 photon counting head, and (b) a C8855-1 photon counting unit. The H11870-09 photon counting head provides a binary signal (0-3.5V) per each photon detected. Hence, is well suited to work in an environment with elevated electro-magnetic noise. Its count sensitivity is shown in FIGURE 4. One of the key reasons for selecting this unit was the low dark count rate (15 pulses/s), to avoid false positives.

As the photon counting head is not to suitable for working in a partial vacuum, three fused silica windows were inserted in the body of the vacuum tank to allow the UV to be radiate from the EUT to the photon counting head that was placed outside the vacuum tank. The transmission curve of

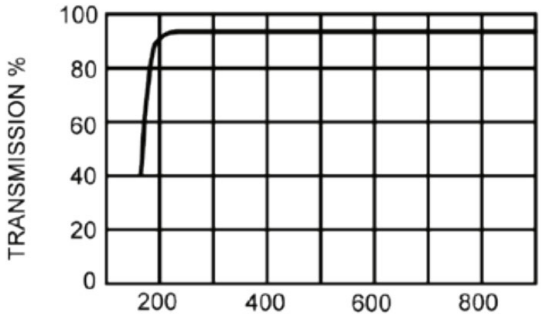

FIGURE 5. Fused silica window transmission curve [25].

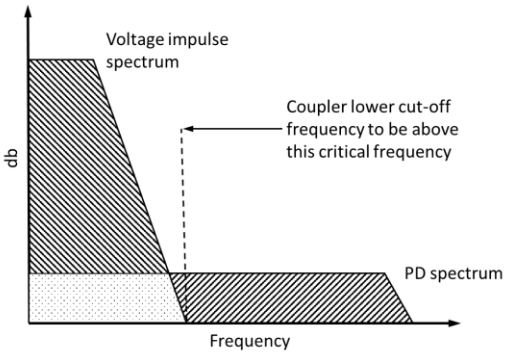

FIGURE 6. Principle of PD detection under inverter voltage impulses using UHF systems (after [26]).

the windows is reported in FIGURE 5. Its choice is based on the evidence that PDs in air emit in the UV range, from 300nm to 400 nm [9].

The use of UHF systems for PD detection is supported by the fact that, in the UHF frequency range, the spectral content of the PD signal exceeds that of the interference from the supply system [20]. This principle is sketched in FIGURE 6, taken from [26], By selecting a UHF sensor with the proper lower cutoff frequency, it is possible to remove the interference while preserving a significant part of the PD signal energy. For the experiments reported in the following, the UHF PD sensor was a Surface Mounting Device (SMD) pass-through, employed as a monopole inside the vacuum cell [27]. The output of the sensor was sent to a Tektronix RSA306B (9 kHz → 6.2 GHz) spectrum analyzer.

For conventional PD detection, a ferrite-core high-frequency current transformer (HFCT) was used to couple the PD signals. An external capacitor (1 nF) was connected in parallel to the twisted pairs to improve the detection sensitivity (better than 5 pC). The PD detector was a Techimp PDBaseII. The PDBaseII has bandwidth 40 MHz, sampling rate 200 MSa/s, and provides the PD pulse waveform [28]. This feature is useful to understand the behavior of PDs at reduced pressure.

III. PD DETECTION SENSITIVITY

Tests were performed to compare the sensitivity of the PD detection systems. Using a high voltage transformer ensures

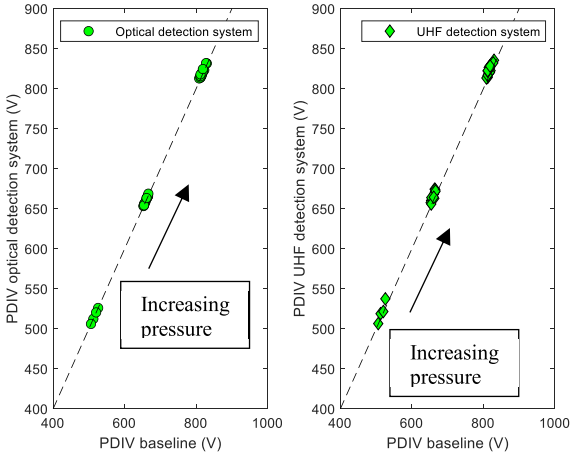

FIGURE 7. Comparison of PDIV values obtained by the standard method based on conducted signals (baseline) and alternative optical and UHF detection systems. Tests performed at 200 mbar, 500 mbar and 1013 mbar.

the lowest interference possible between PD signals and the source. Therefore, all detection systems operate with the highest sensitivity [29].

Under repetitive voltage impulses, due to the interference from the high voltage source, detection of conducted signals is impossible. UHF sensors are employed for this purpose [20]. But, depending on the atmospheric pressure, detection using UHF sensors might be unfeasible as the PD pulses lose frequency content [18], [19].

To compare the sensitivity of the different sensors, the baseline is the PDIV obtained using conducted signals under 50 Hz sinusoidal voltage waveforms (highest sensitivity). It is important to note that:

- Reducing the gas pressure might improve the detection sensitivity of the optical sensor due to the lower absorbance of the air.
- At low pressures, the frequency content of the PD pulse is low [18], hampering PD detection in the UHF range. This is related to the discharge typology. At high pressure, PD are streamer discharges having large frequency content. At low pressures, PD are Townsend discharges with low frequency content [30].

FIGURE 7 indicates that the optical and the conventional detection systems provide the same PDIV values at all pressures. Indeed, decreasing the pressure the optical detection system improves its sensitivity. FIGURE 8 highlights that the number of photons observed per unit time at 1.2 × PDIV increases at low pressures [31]. This indicates that detecting PDs becomes easier at low pressures, probably due to the reduced absorbance of the air. In the tests reported in FIGURE 8, the minimum pressure is 25 mbar. This value is much lower than those typical of aircraft cruising altitudes: it was selected to emphasize the results.

The detection sensitivity of the UHF sensor is affected by low pressures. This is not hampering measurements under sinusoidal waveforms as shown in FIGURE 7 but can be an issue under inverter voltage waveforms. FIGURE 9 shows the spectrum of the inverter interference in the absence and in the

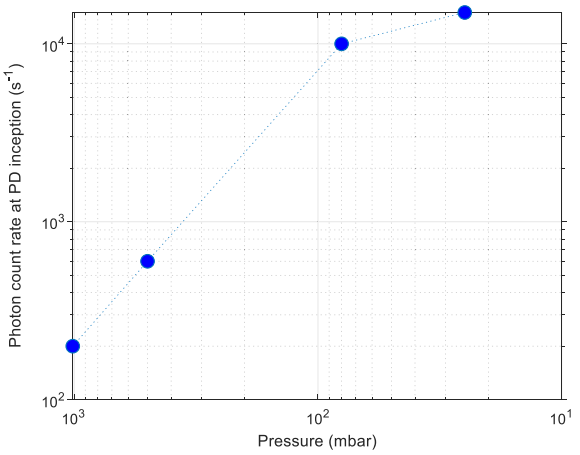

FIGURE 8. Photon count rate in the presence of PD activity as a function of pressure (50 Hz sinusoidal voltage, constant overvoltage ratio). Since the PDIV is correlated with pressure, tests were carried out keeping constant the ratio of the applied voltage to the PD inception voltage (120% in the experiments).

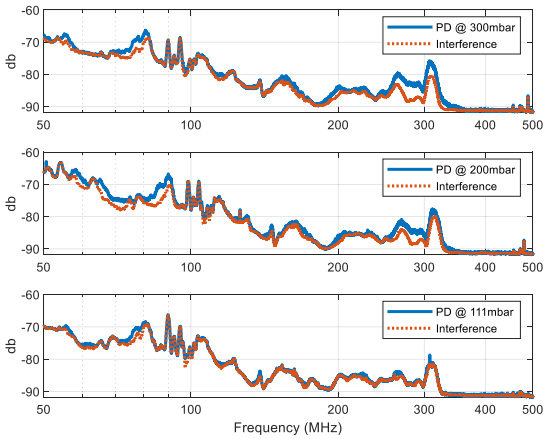

FIGURE 9. Spectra of the signals received by the UHF sensors at 300 mbar, 200 mbar and 100 mbar.

presence of PDs. PD can be detected easily above 250 MHz at 300 mbar. At 200 mbar detection becomes more difficult. At 100 mbar PD detection is no longer possible.

IV. RESULTS

In the following, tests at various pressures will be discussed. The pressures were selected to get a thorough picture, reaching values well below those experienced by commercial aircraft. Before discussing the results, it is important to highlight how PDIV tests were carried out and the influence of pressure on PDIV measurement. The voltage was raised in steps of 25 V, whose durations increase as the pressure decrease (see Table 1). This choice comes from the fact that two conditions must be met to start a PD: (1) the voltage should exceed the PDIV and (2) a free electron should be available. Free electrons are created by photoionization of the gas molecules [32] and might appear after the PDIV has been reached. Thus, there might be a significant (positive) error in the measured PDIV if the rate of voltage raise is too large. This is likely to happen at low pressures, as the photoionization probability scales with the number density of the gas.

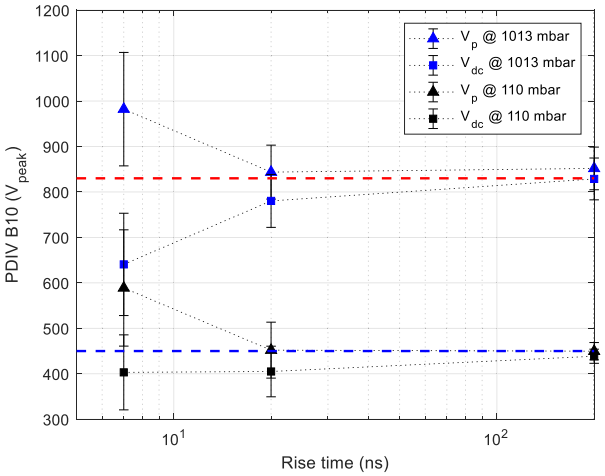

FIGURE 10. PDIV values obtained changing the rise time at 1013 mbar and 110 mbar. Switching frequency: 10 kHz. Sensor: optical. All measurements performed at room temperature.

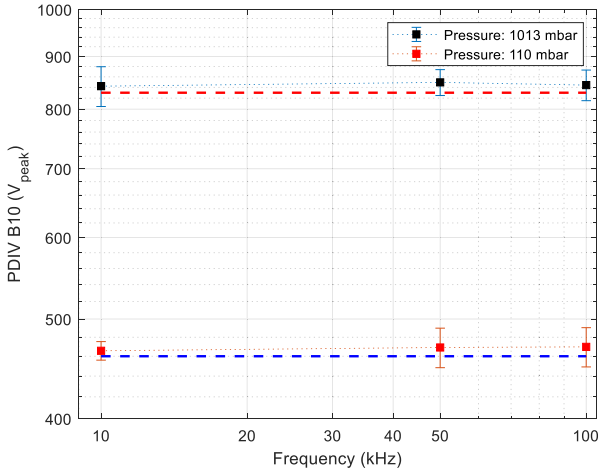

FIGURE 11. PDIV as a function of frequency. The measurement was carried out using voltage impulses with rise time 7 ns. The readings are expressed in terms of the peak voltage, corrected by a factor equal to 0.75 inferred from FIGURE 10. Sensors: optical. All measurements performed at room temperature.

TABLE 1. Duration of voltage steps used for PDIV measurements.

Pressure (mbar)	1013	507	111	82	50	25
Duration (min)	0.5	1	5	8	10	20

A. DEPENDENCE OF PDIV ON VOLTAGE IMPULSE REPETITION FREQUENCY AND RISE TIME

The PDIV depends on the voltage waveform in two ways. On one side, the voltage waveform influences the distribution of the voltage within the test object. On the other side, the waveform of the potential difference between two points of the insulation might influence the physics of the discharge at a microscopic level.

Since the first problem has been addressed several times in literature (see e.g [33]–[35]), focus will be given here to the second problem, which can be summarized as follows. Let two points of the winding be subjected to voltage waveforms having the same peak voltage but different rise times or frequencies. Will one waveform be able to start PD activity at a lower peak voltage level?

To answer empirically to the above question, the PDIV was measured with different repetition frequencies and rise times. Tests were carried out at two different pressures (1013 mbar and 110 mbar), at room temperature.

The first test was performed keeping a constant frequency of 10 kHz and variable rise times. Three rise times were selected, the two shortest ones (7 ns and 15 ns) are representative of WBG devices, whereas the largest one (150 ns) is representative of devices using conventional silicon switches. Results from tests using 50 Hz sinusoidal voltages were used as a baseline.

The experimental results are depicted in FIGURE 10, which reports both the peak voltage and the corresponding DC bus voltage. Inspecting FIGURE 10 one can conclude that the measured PDIV values are centered around the values observed at 50 Hz, thus that the rise time has a negligible effect. The larger fluctuations associated with the shortest rise time (7 ns) can be explained considering the large overshoot of the voltage waveform (see FIGURE 1) through the reasoning exposed in Appendix A.

Since the results in FIGURE 10 were obtained with a single switching frequency (10 kHz), PDIV measurements obtained with the minimum rise time (7 ns) and increasing the switching frequency up to 100 kHz were carried out as well. FIGURE 11 shows that the PDIV is independent of the switching frequency. A simple framework to interpret and justify these results is reported in Appendix B.

It is worthwhile to observe that [17] reports a marked dependence of PDIV on frequency. However, the results reported in [17] are based on experiments performed on a point/plane configuration in air. For this type of setup, the diffusion of ions in proximity of the point plays a very important role, and its effects are highly dependent on the ratio between the diffusion time constant and the period of the voltage.

B. DEPENDENCE OF PDIV ON PRESSURE AND TEMPERATURE

To derive an analytical model to predict PDIV as a function of pressure, several pressure levels were tested, including levels lower than those experienced by commercial aircraft. All tests were performed at room temperature using both 50 Hz AC and inverter voltages (using the shortest rise time).

The curves obtained using sinusoidal voltages show a minimum in the range 50÷70 mbar (see FIGURE 12). Despite the resemblance, the Paschen curve is not apt to perfectly reproduce the dependence of PDIV data on pressure. In particular, the minimum is higher than what predicted using the Paschen curve. This was observed already in [14].

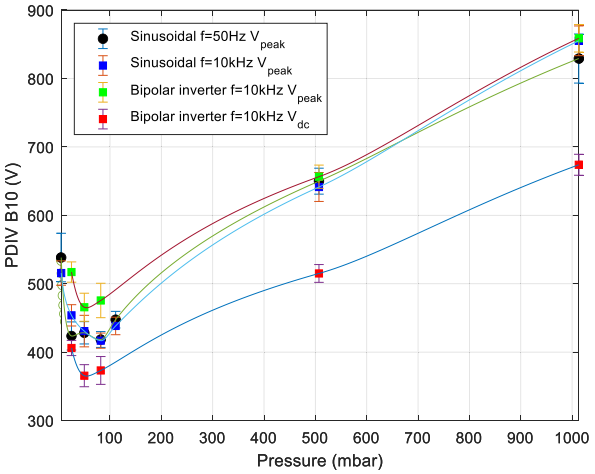

FIGURE 12. PDIV values obtained using different supply voltage waveforms as a function of pressure. The inverter rise time in these tests was 7 ns, the switching frequency 10 kHz. Sensors: optical for tests using inverter waveforms, hfct and optical for tests using sinusoidal waveforms. All measurements performed at room temperature.

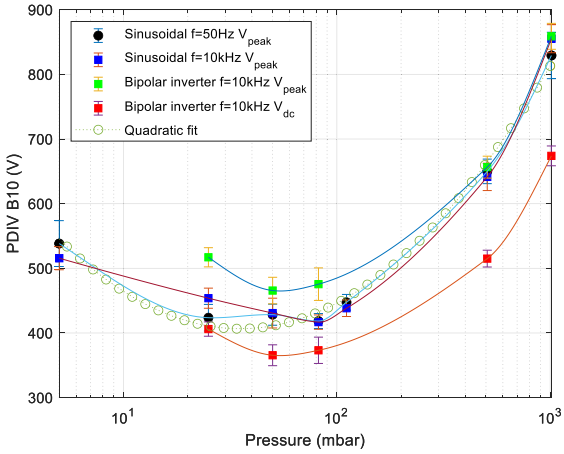

FIGURE 13. PDIV values obtained using different supply voltage waveforms as a function of pressure (semi-log axis). The inverter rise time in these tests was 7 ns, the switching frequency 10 kHz.. Sensors: optical for tests using inverter waveforms, hfct and optical for tests using sinusoidal waveforms. All measurements performed at room temperature.

If the same data are plotted as a function of the logarithm of the pressure, a nearly quadratic behavior can be observed (see FIGURE 13). Using linear regression, an empirical model based on the logarithm of the pressure (in bar) was fitted to the data measured under AC 50 Hz sinusoidal voltages:

$$\begin{aligned} PDIV(p) &= 813 + 243 \ln p + 36.3 (\ln p)^2 \\ &= 813 \left(1 + 0.299 \ln p + 0.0446 (\ln p)^2\right) \end{aligned} \quad (1)$$

The model provides a good approximation of the measured data at all pressure levels. The curves obtained using the bipolar inverter have a behavior like the curves obtained using sinusoidal voltages. Similarly to FIGURE 10, if the peak voltage is reported, they are constantly above those relevant to the sinusoidal voltage. Otherwise, if the DC bus voltage is reported, they are below indicating that the PDIV is not influenced by the voltage waveform features.

C. DEPENDENCE OF PDIV ON BOTH PRESSURE AND TEMPERATURE

To evaluate the dependence of PDIV on both pressure and temperature, additional tests were carried out at 120 °C, at different pressure levels. Since ionization processes depend on the mean free path which is inversely related to the number density (number of gas molecules per cubic meter), the results of the tests can be reported as a function of the number density $n_{P,T}$:

$$n_{P,T} = \frac{P}{1.38066 \times 10^{-23} T} \tag{2}$$

where P is the pressure (in Pa) and T the temperature (in K). If n_{ref} is the number density, corresponding to the pressure (P_{ref}) and temperature (T_{ref}) at which PDIV measurement were carried out in the lab, (1) can be normalized as follows:

$$\frac{PDIV_{P,T}}{PDIV_{ref}} = 1 + 0.299 \ln\left(\frac{n_{P,T}}{n_{ref}}\right) + 0.0446 \ln\left(\frac{n_{P,T}}{n_{ref}}\right)^2 \tag{3}$$

where $PDIV_{ref}$ is the PDIV measured in the lab at the reference pressure and temperature, $PDIV_{P,T}$ is the estimate of the PDIV at the desired temperature and pressure.

To assess the effectiveness of model (3), the number density was normalized to that at 25°C, 1013 mbar and all experimental data (at 25°C and 140°C) were reported in FIGURE 14. As can be seen, there is a very good agreement between the experimental data and the prediction achieved by (3), indicating that, for the considered insulation system, the dominant factor for PDIV is the density of the gas.

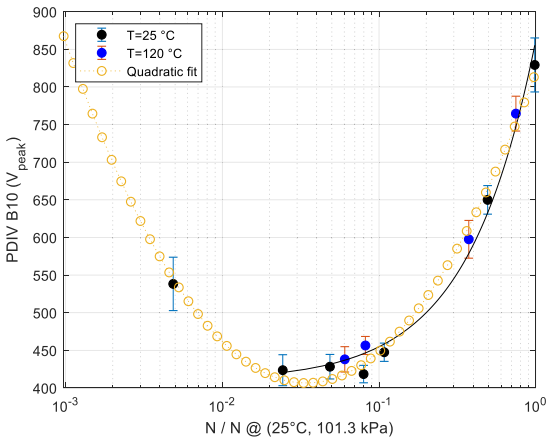

FIGURE 14. PDIV values obtained using 50 Hz sinusoidal waveforms at 25°C and 120 °C. The solid line represents the line fitting both data sets as a function of the air number density. The predictions achieved through the quadratic model (3) are also reported. Sensor: hfct and optical.

Using (2), the model (3) can be simplified introducing the reference pressure and temperature:

$$\frac{PDIV_{P,T}}{PDIV_{ref}} = 1 + 0.299 \ln\left(\frac{P}{P_{ref}}\frac{T_{ref}}{T}\right) + 0.0446 \ln\left(\frac{P}{P_{ref}}\frac{T_{ref}}{T}\right)^2 \tag{4}$$

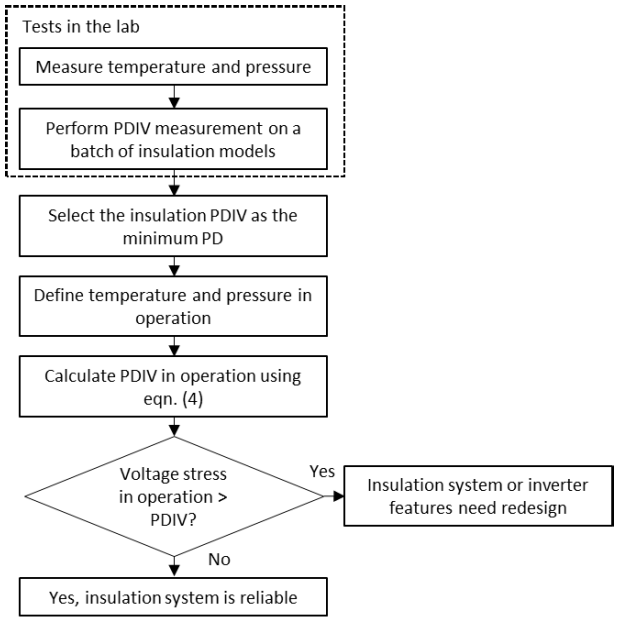

FIGURE 15. Flowchart to evaluate the PDIV at operating conditions starting from lab measurements.

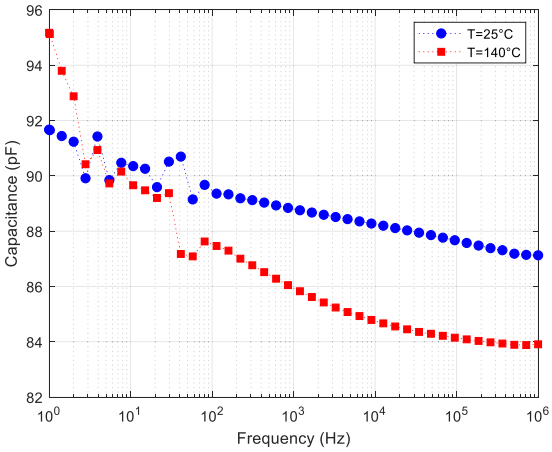

FIGURE 16. Capacitance of a coil at 25 °C and 140 °C as a function of frequency.

The procedure to estimate the PDIV as a function of pressure and temperature starting from measurements performed at the reference condition is synthetized in FIGURE 15

The good performance of model (3) seems to rule out other factors that might affect the PDIV. One of these factors, is the dependency of the permittivity of the solid dielectric on temperature [36]. To test whether the permittivity could be influenced by the temperatures used in these experiments, the winding wire was wound on a copper support to create a coil. To minimize inductive effects, two layers of wire were wound around the support: clockwise and counterclockwise. The coil was placed in the oven and connected using silicone unshielded cables to a Novocontrol alpha-beta analyzer. FIGURE 16 shows the coil capacitance as a function of frequency and for two different temperatures:

25°C and 140°C. As can be seen, the difference between the capacitance values is negligible, confirming the previous hypothesis.

This result could be expected for a winding wire since the polyamide-imide enamel have glass transition temperature well above the test temperatures used here (e.g. 275 °C for Solvay Torlon, [37]) and, therefore, the dependence of the relative permittivity on temperature is limited. Insulation systems with lower glass temperatures, based e.g. on epoxies, can have a much marked dependence on temperature, as observed in [16].

D. IS IT POSSIBLE TO GENERALIZE THE MODEL?

Demonstrating in an analytical way the generality of the model presented in the previous Section seems to be very complicated. The form of the model (equation (1) or (4)) does not suggest that it can be obtained analytically in a straightforward way. One should bear in mind that the model fits data coming from discharges that shift from streamer to Townsend discharges as the pressure is reduced (thus, two different inception criteria are needed). In the following, an indirect proof of its generality will be presented for the range of air densities that is typical of commercial aircraft.

In [38], a software for estimating the PDIV in twisted pairs is presented. The model is based on the application of the streamer inception criterion. Thus, it does not work at very low pressures where Townsend discharges dominate. The streamer inception criterion assumes that there exists a critical number of electrons in the head of an avalanche (N_{cr}) that will turn the avalanche into a streamer. Using the Townsend effective ionization coefficient α_e one obtains [39]:

$$\exp\left(\int_0^{l_{cr}} \alpha_e\left(E\left(x\right)\right) \mathrm{d}x\right) = N_{cr} \rightarrow \int_0^{l_{cr}} \alpha_e\left(E\left(x\right)\right) \mathrm{d}x = K \tag{5}$$

where l_{cr} is the length of the field line where the discharge develops. In practice, assuming that K is known, one should evaluate equation (5) for all field lines in the geometry at different voltages. The lowest voltage that permits to satisfy equation (5) is the PDIV.

The software proposed in [38] resorts to the FEM software package COMSOL to solve the electrostatic problem (calculation of $E(x)$ and field lines), and on the Bolsig software [40] to determine α_e as a function of the electric field and the pressure. Since K depends on the length of the field line [41], the model was trained fitting PDIV values measured on several different wires. The PDIV tests to determine K were carried out in the lab, at room temperature and pressure. It was proven that, using $K = 6$, the model can predict, with an error lower than 10%, the PDIV of the same wires at different temperatures and pressures [38].

To check whether the model (4) can be generalized, simulations were carried out using the software to predict the PDIV of wires of different diameters and thicknesses. The results are reported in FIGURE 17. As can be seen, the software shows some fluctuations that are associated to the estimate of the electric field lines lengths provided by CONSOL (the software is currently being ported under FEMM to achieve a better control of the electrical field lines). Despite that, the quadratic model in equation (4) can predict in a good way the trend of PDIV as a function of the air density. Therefore, it can be considered a simple yet effective way of estimating the behavior of the insulation at cruising altitudes, at least for simple geometries with mildly divergent electrical fields as those existing in the turn/turn insulation.

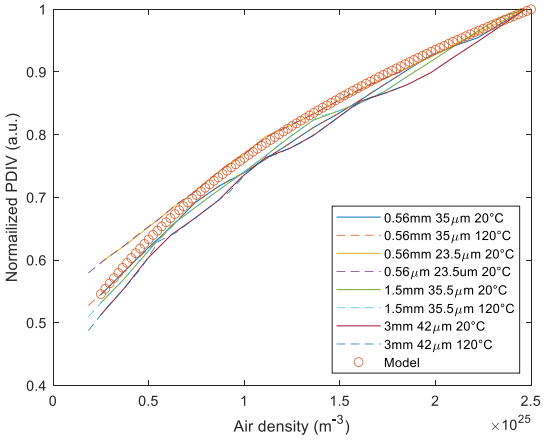

FIGURE 17. PDIV simulations for wires having various diameters and dielectric thicknesses compared with results provided by model (3).

V. CONCLUSION

Considering its practical implications, the most important result of the experiments presented in this paper is that the PDIV of winding wires is the same using SiC voltage impulses or 50 Hz sinusoidal waveforms. This implies that only the peak value of the turn/turn voltage is important, whereas the impulse voltage rise time and the switching frequency do not affect PDIV significantly. This is a key finding, as it supports using 50 Hz sinusoidal waveforms or impulse voltages with moderate slew rates to test insulation systems.

The paper has also presented an analytical model to predict the PDIV as a function of both temperature and pressure. The model can be used to predict the turn/turn insulation PDIV starting from measurements performed at standard conditions (1013 mbar and 25°C, for example) and evaluates the evolution of PDIV in operation (150 mbar and 120°C, for example) as a function of the gas number density only. This model might not be valid for insulation systems having a glass transition temperature close to the operating temperature. In that case, the contribution of the permittivity increase at high temperatures should be accounted for as a separate factor.

.

APPENDIX A EFFECT OF VOLTAGE OVERSHOOT ON PDIV MEASUREMENT

PDIV is the result of the measurement of the minimum voltage able to ignite PD (V_{inc}) in an insulation system. Explaining the differences between PDIV measured using sinusoidal voltages and impulse voltages having a large overshoot factor starts from recalling the conditions for PD ignition: (a) the instantaneous voltage, v(t), exceeds V_{inc}, and (b) a free electron is available to start the avalanche. Consider FIGURE 18, if the peak voltage of the waveform is equal to V_{inc} (dashed line), the PD inception probability is zero since the probability that a starting electron is available at the time $v(t) = V_{inc}$ is also equal to zero. If the peak voltage exceeds V_{inc}, the discharge can happen at all voltages satisfying $v(t) \geq V_{inc}$ (highlighted by the shaded area). The larger the overvoltage, the larger the probability that, in a single cycle, the PD is ignited. If the peak voltage is reported, the measured value is always larger than V_{inc}. Otherwise, if the DC bus voltage is reported, it is always lower than V_{inc}.

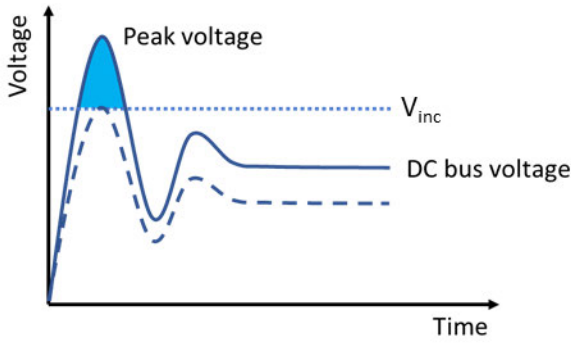

FIGURE 18. Sketch of the process of PD inception using repetitive impulse voltages. The shaded area highlights the voltage levels above PDIV, where PD can take place if a starting electron is available.

The same type of error affects measurement with sinusoidal waveforms. However, considering the low derivatives of sinusoidal waveforms at industrial frequency (50/60 Hz), the error is much less important as, for a given overvoltage, the voltage stays above V_{inc}. for a much longer time. Thus, 50 Hz AC measurements were considered as the baseline for comparison.

APPENDIX B THEORETICAL CONSIDERATIONS REGARDING THE EFFECTS OF VOLTAGE WAVEFORM ON PDIV

Despite the fact that the results reported in FIGURE 10 and FIGURE 11 show that the effects of voltage waveform rise time and switching frequency on PDIV are negligible, it is worth trying to analyze in general terms the physics of the underlying phenomena. One must thus consider the relationship between the applied voltages and the corresponding electric field waveforms, which can be best appreciated in the frequency domain.

The solid insulation and the gas can be regarded as two capacitors in series. If the permittivity of the solid insulation (wire enamel) does not depend on the frequency, the system is algebraic and the field in the gas is a scaled replica of the applied voltage waveform.

However, dielectrics are generally dynamic systems and their permittivity shows a dependence on frequency as dipole orientation will cease to occur above some critical frequency, f_c, [36]. If the f_c of the winding wire insulation is in the range of frequencies where the spectral energy of the voltage waveform is non-negligible, above the critical frequency the permittivity mismatch between air and solid decreases. Compared with the ideal case of constant permittivity, the electric field will not be a scaled replica of the voltage waveform but, since at higher frequencies the field in the air will be lower, one can expect that the peak of the field will be lower and the PDIV higher.

The distortion of the electric field waveform might be visible going from long rise times (low frequency content) to short rise times (low frequency content) as an increase of PDIV. This was not observed in the experiments discussed in Section IV, using state-of-the-art SiC inverters with a spectral content of the voltage up to 30 MHz for the shortest rise times [21]. However, the field distortion might be observed in the future when more performant devices (based e.g. on GaN) will become available.

Regarding the effect of frequency, one can approach the problem mathematically. The Fourier series of a periodic signal corresponds to the Fourier transforms of a single period (aperiodic signal) sampled at frequencies multiple of the repetition frequency (the switching frequency in this case) [42]. Thus, changing the switching frequency, the ratio of the spectral energies in different frequency ranges might change, but only in a very limited way. This reasoning is confirmed by the empirical evidence that switching frequency does not alter appreciably the PDIV

REFERENCES

[1] J. Benzaquen, F. Fateh, M. B. Shadmand, and B. Mirafzal, "Performance comparison of active rectifier control schemes in more electric aircraft applications," *IEEE Trans. Transport. Electrific.*, vol. 5, no. 4, pp. 1470–1479, Dec. 2019, doi: 10.1109/TTE.2019.2940847.

[2] A. Nawawi, R. Simanjorang, C. J. Gajanayake, A. K. Gupta, C. F. Tong, S. Yin, A. Sakanova, Y. Liu, Y. Liu, M. Kai, K. Y. See, and K.-J. Tseng, "Design and demonstration of high power density inverter for aircraft applications," *IEEE Trans. Ind. Appl.*, vol. 53, no. 2, pp. 1168–1176, Mar. 2017, doi: 10.1109/TIA.2016.2623282.

[3] S. Yin, K. J. Tseng, R. Simanjorang, Y. Liu, and J. Pou, "A 50-kW high-frequency and high-efficiency SiC voltage source inverter for more electric aircraft," *IEEE Trans. Ind. Electron.*, vol. 64, no. 11, pp. 9124–9134, Nov. 2017, doi: 10.1109/TIE.2017.2696490.

[4] C. Degoutte, O. Sanchez, J. Renaudin, N. Boukari, P. Decroux, and J. D. Salvany, "Aircraft 270 VDC power distribution improvements using wide band gap semi-conductors," in *Proc. Int. Conf. Electr. Syst. Aircr., Railway, Ship Propuls. Road Vehicles Int. Transp. Electrific. Conf. (ESARS-ITEC)*, Nov. 2016, pp. 1–6, doi: 10.1109/ESARS-ITEC.2016.7841357.

[5] E. Persson, "Transient effects in application of PWM inverters to induction motors," in *Proc. Conf. Rec. Annu. Pulp Paper Ind. Tech. Conf.*, Jun. 1991, pp. 228–233, doi: 10.1109/PAPCON.1991.239644.

[6] M. Melfi, A. M. J. Sung, S. Bell, and G. L. Skibinski, "Effect of surge voltage risetime on the insulation of low-voltage machines fed by PWM converters," *IEEE Trans. Ind. Appl.*, vol. 34, no. 4, pp. 766–775, Jul. 1998, doi: 10.1109/28.703971.

[7] Y. Xie, J. Zhang, F. Leonardi, A. R. Munoz, M. W. Degner, and F. Liang, "Voltage stress modeling and measurement for random-wound windings driven by inverters," in *Proc. IEEE Int. Electric Mach. Drives Conf. (IEMDC)*, May 2019, pp. 1917–1924, doi: 10.1109/IEMDC.2019.8785133.

[8] M. Pastura, S. Nuzzo, G. Franceschini, G. Sala, and D. Barater, "Sensitivity analysis on the voltage distribution within windings of electrical machines fed by wide band gap converters," in *Proc. Int. Conf. Electr. Mach. (ICEM)*, Gothenburg, Sweden, Aug. 2020, pp. 1594–1600.

[9] *High-Voltage Test Techniques—Partial Discharge Measurements*, IEC Standard 60270, 2015.

[10] M. Kaufhold, H. Aninger, M. Berth, J. Speck, and M. Eberhardt, "Electrical stress and failure mechanism of the winding insulation in PWM-inverter-fed low-voltage induction motors," *IEEE Trans. Ind. Electron.*, vol. 47, no. 2, pp. 396–402, Apr. 2000, doi: 10.1109/41.836355.

[11] W. Yin, "Failure mechanism of winding insulations in inverter-fed motors," *IEEE Elect. Insul. Mag.*, vol. 13, no. 6, pp. 18–23, Nov. 1997, doi: 10.1109/57.637150.

[12] G. Stone, S. Campbell, and S. Tetreault, "Inverter-fed drives: Which motor stators are at risk?" *IEEE Ind. Appl. Mag.*, vol. 6, no. 5, pp. 17–22, Sep. 2000, doi: 10.1109/2943.863631.

[13] *Rotating Electrical Machines—Part 18-41: Partial Discharge Free Electrical Insulation Systems (Type I) Used in Rotating Electrical Machines Fed From Voltage Converters–Qualification and Quality Control Tests*, IEC Standard. 60034-18-41, 2019.

[14] G. G. Karady, M. D. Sirkis, and L. Liu, "Investigation of corona initiation voltage at reduced pressures," *IEEE Trans. Aerosp. Electron. Syst.*, vol. 30, no. 1, pp. 144–150, Jan. 1994, doi: 10.1109/7.250415.

[15] R. Rui and I. Cotton, "Impact of low pressure aerospace environment on machine winding insulation," in *Proc. IEEE Int. Symp. Electr. Insul.*, Jun. 2010, pp. 1–5, doi: 10.1109/ELINSL.2010.5549718.

[16] Y. Wang, X. Yi, Y. Wang, X. Zhang, Y. Yin, T. Han, and K. S. Haran, "Partial-discharge-free insulation design of air-core permanent magnet synchronous machine for aircraft propulsion," *IEEE Trans. Transport. Electrific.*, early access, May 4, 2020, doi: 10.1109/TTE.2020.2992052.

[17] A. N. Esfahani, S. Shahabi, G. Stone, and B. Kordi, "Investigation of corona partial discharge characteristics under variable frequency and air pressure," in *Proc. IEEE Electr. Insul. Conf. (EIC)*, Jun. 2018, pp. 31–34, doi: 10.1109/EIC.2018.8481047.

[18] A. Cavallini, L. Versari, and L. Fornasari, "Feasibility of partial discharge detection in inverter-fed actuators used in aircrafts," in *Proc. Annu. Rep. Conf. Electr. Insul. Dielectr. Phenomena*, Oct. 2013, pp. 1250–1253, doi: 10.1109/CEIDP.2013.6748115.

[19] C. Abadie, T. Billard, and T. Lebey, "Influence of pressure on partial discharge spectra," in *Proc. IEEE Electr. Insul. Conf. (EIC)*, Jun. 2016, pp. 507–510, doi: 10.1109/EIC.2016.7548648.

[20] D. Fabiani, A. Cavallini, and G. C. Montanari, "A UHF technique for advanced PD measurements on inverter-fed motors," *IEEE Trans. Power Electron.*, vol. 23, no. 5, pp. 2546–2556, Sep. 2008, doi: 10.1109/TPEL.2008.2002069.

[21] D. R. Meyer, A. Cavallini, L. Lusuardi, D. Barater, G. Pietrini, and A. Soldati, "Influence of impulse voltage repetition frequency on RPDIV in partial vacuum," *IEEE Trans. Dielectr. Electr. Insul.*, vol. 25, no. 3, pp. 873–882, Jun. 2018, doi: 10.1109/TDEI.2018.006722.

[22] J. Jiang, K. Wang, L. Chen, I. Cotton, J. Chen, J. Chen, and C. Zhang, "Optical sensing of partial discharge in more electric aircraft," *IEEE Sensors J.*, vol. 20, no. 21, pp. 12723–12731, Nov. 2020, doi: 10.1109/JSEN.2020.3002881.

[23] *Winding Wires–Test Methods—Part 5: Electrical Properties*, IEC Standard 60851-5, 2008.

[24] Hamamatsu. *Photon Counting Head 811H70 Series*. Accessed: Jul. 3, 2020. [Online]. Available: https://www.hamamatsu.com/resources/pdf/etd/H11870_TPMO1061E.pdf

[25] Torr Scientific Ltd. (Mar. 7, 2020). *Vacuum Optics*. [Online]. Available: http://torrscientific.co.uk/wp-content/uploads/2018/12/Vacuum-Optics-Catalogue.pdf

[26] *Electrical Insulating Materials and Systems–Electrical Measurement of Partial Discharges (PD) Under Short Rise Time and Repetitive Voltage Impulses*, Standard IEC TS 61934, 2011.

[27] T. Billard, T. Lebey, and F. Fresnet, "Partial discharge in electric motor fed by a PWM inverter: Off-line and on-line detection," *IEEE Trans. Dielectr. Electr. Insul.*, vol. 21, no. 3, pp. 1235–1242, Jun. 2014, doi: 10.1109/TDEI.2014.6832270.

[28] A. Contin, A. Cavallini, G. C. Montanari, G. Pasini, and F. Puletti, "Digital detection and fuzzy classification of partial discharge signals," *IEEE Trans. Dielectr. Electr. Insul.*, vol. 9, no. 3, pp. 335–348, Jun. 2002, doi: 10.1109/TDEI.2002.1007695.

[29] *High Voltage Test Techniques–Measurement of Partial Discharges by Electromagnetic and Acoustic Methods*, Standard IEC TS 62478, 2016.

[30] P. Osmokrovic, I. Krivokapic, and S. Krstic, "Mechanism of electrical breakdown left of paschen minimum," *IEEE Trans. Dielectr. Electr. Insul.*, vol. 1, no. 1, pp. 77–81, Feb. 1994, doi: 10.1109/94.300234.

[31] L. Lusuardi, A. Rumi, G. Neretti, P. Seri, and A. Cavallini, "Assessing the severity of partial discharges in aerospace applications," in *Proc. IEEE Conf. Electr. Insul. Dielectr. Phenomena (CEIDP)*, Oct. 2019, pp. 267–270, doi: 10.1109/CEIDP47102.2019.9009970.

[32] L. Niemeyer, "A generalized approach to partial discharge modeling," *IEEE Trans. Dielectr. Electr. Insul.*, vol. 2, no. 4, pp. 510–528, Aug. 1995, doi: 10.1109/94.407017.

[33] G. Suresh, H. A. Toliyat, D. A. Rendusara, and P. N. Enjeti, "Predicting the transient effects of PWM voltage waveform on the stator windings of random wound induction motors," *IEEE Trans. Power Electron.*, vol. 14, no. 1, pp. 23–30, Jan. 1999, doi: 10.1109/63.737589.

[34] C. Petrarca, A. Maffucci, V. Tucci, and M. Vitelli, "Analysis of the voltage distribution in a motor stator winding subjected to steep-fronted surge voltages by means of a multiconductor lossy transmission line model," *IEEE Trans. Energy Convers.*, vol. 19, no. 1, pp. 7–17, Mar. 2004, doi: 10.1109/TEC.2003.821834.

[35] V. Mihaila, S. Duchesne, and D. Roger, "A simulation method to predict the turn-to-turn voltage spikes in a PWM fed motor winding," *IEEE Trans. Dielectr. Electr. Insul.*, vol. 18, no. 5, pp. 1609–1615, Oct. 2011, doi: 10.1109/TDEI.2011.6032831.

[36] F. Kremer and A. Schönhals, *Broadband Dielectric Spectroscopy*. Berlin, Germany: Springer, 2003.

[37] *Torlon-PAI-Design-Guide_EN-227547.pdf*. Accessed: Nov. 18, 2020. [Online]. Available: https://www.solvayultrapolymers.com/en/binaries/Torlon-PAI-Design-Guide_EN-227547.pdf

[38] L. Lusuardi, A. Cavallini, M. G. de la Calle, J. M. Martinez-Tarifa, and G. Robles, "Insulation design of low voltage electrical motors fed by PWM inverters," *IEEE Elect. Insul. Mag.*, vol. 35, no. 3, pp. 7–15, May 2019, doi: 10.1109/MEI.2019.8689431.

[39] A. Pedersen, "On the electrical breakdown of gaseous dielectrics—An engineering approach," *IEEE Trans. Electr. Insul.*, vol. 24, no. 5, pp. 721–739, Oct. 1989, doi: 10.1109/14.42156.

[40] *LXCAT*. Accessed: Jul. 3, 2020. [Online]. Available: https://us.lxcat.net/home/

[41] N. Malik, "Streamer breakdown criterion for compressed gases," *IEEE Trans. Electr. Insul.*, vol. EI-16, no. 5, pp. 463–467, Oct. 1981, doi: 10.1109/TEI.1981.298444.

[42] R. N. Bracewell, *The Fourier Transform and Its Applications*, 2nd ed. New York, NY, USA: McGraw-Hill, 1986.

LUCA LUSUARDI (Member, IEEE) was born in September 1991. He received the B.Sc. degree in energy engineering, the M.Sc. degree in energy and nuclear engineering, and the Ph.D. degree in biomedical, electrical and systems engineering from the University of Bologna, in 2013, 2016, and 2019, respectively. He joined the IEEE Dielectrics and Electrical Insulation Society, in June 2017. Since 2019, he has been a Visiting Researcher with the University of Nottingham, U.K. Since December 2019, he has been working with Rhiva AG (born from a detachment of the E-mobility group of Thyssenkrupp Presta AG), Research and Development Team as the responsible of electrical insulation of electric powertrains. His research interests include design, analysis and thermal management of electrical machines and drives, diagnosis of insulation systems by partial discharge analysis, and reliability modeling of inverter-fed low voltage motors.

ALBERTO RUMI (Student Member, IEEE) was born in Lugo (RA), Italy, in April 1994. He received the B.Sc. and M.S. degrees in electrical engineering from the University of Bologna, Italy, in July 2016 and March 2019, respectively, where he is currently pursuing the Ph.D. degree in biomedical, electrical and systems engineering. His research interests include diagnosis of insulation systems by partial discharge analysis, the study of the ageing mechanisms of rotating electrical machines and reliability of inverter-fed low voltage motors, especially in the aeronautical and automotive fields.

ANDREA CAVALLINI (Senior Member, IEEE) was born in December 1963. He received the master's and Ph.D. degrees in electrical engineering from the University of Bologna, in 1990 and 1995, respectively. From 1995 to 1998, he was a Researcher with Ferrara University. Since 1998, he has been an Associate Professor with Bologna University. He was a Co-founder of spinoff company Techimp HQ Spa. He is a Project Leader of the IEC 60034-18-41 Ed. 2. He is the author or coauthor of more than 250 international articles and holds 16 international patents. His research interests include diagnosis of insulation systems by partial discharge analysis, reliability of electrical systems, and artificial intelligence. He is a member of the IEC TC 2/MT 10.

DAVIDE BARATER (Member, IEEE) received the master's degree in electronic engineering and the Ph.D. degree in information technology from the University of Parma, Italy, in 2009 and 2014, respectively.

He was an Honorary Scholar with the University of Nottingham, U.K., in 2012, and a Visiting Researcher with the University of Kiel, in 2015. He is currently an Assistant Professor with the Department of Engineering Enzo Ferrari, University of Modena and Reggio Emilia, Italy. He is the author or coauthor of more than 60 international articles. His research interests include power electronics for e-mobility and motor drives. He is the Coordinator of two European Project, such as RAISE, that evaluates the impact of the high voltage gradients, introduced by the fast commutations of new wide bandgap power devices (SiC, GaN), on the life time of electrical motor insulation systems and AUTO-MEA, that aims to develop electrical motors and drives for next generation of electrical mobility. In particular, novel solutions for windings structures and cooling systems for improved power density, efficiency, and increased frequency operation.

Dr. Barater is an Associate Editor of the IEEE TRANSACTIONS ON INDUSTRY APPLICATIONS.

STEFANO NUZZO (Member, IEEEE) received the B.Sc. and M.Sc. degrees in electrical engineering from the University of Pisa, Pisa, Italy, in 2011 and 2014, respectively, and the Ph.D. degree in electrical engineering from the University of Nottingham, Nottingham, U.K., in 2018.

He worked as a Research Fellow within the Power Electronics, Machines and Control (PEMC) Group, University of Nottingham. Since January 2019, he has been a Research Fellow with the Department of Engineering Enzo Ferrari, University of Modena and Reggio, Modena, Italy. He is also involved in a number of projects related to the more electric aircraft initiative and associated fields. His research interests include analysis, modeling, and optimizations of electrical machines, with focus on salient-pole synchronous generators and brushless excitation systems for industrial power generation applications. He is a member of the IEEE Industrial Electronics Society (IES) and the IEEE Industry Applications Society (IAS). He constantly serves the scientific community as a Reviewer for several journals and conferences.